Detection of range migrating targets in compound-Gaussian clutter

Petrov, Nikita; le Chevalier, Francois; Yarovoy, Alexander

DOI
10.1109/TAES.2017.2731558

Publication date
2018

Document Version
Final published version

Published in
IEEE Transactions on Aerospace and Electronic Systems

Detection of Range Migrating Targets in Compound-Gaussian Clutter

NIKITA PETROV
FRANÇOIS LE CHEVALIER
ALEXANDER G. YAROVOY, Fellow, IEEE
Delft Technical University, Delft, The Netherlands

This paper deals with the problem of coherent radar detection of fast-moving targets in a high-range resolution mode. In particular, we are focusing on the spiky clutter modeled as a compound Gaussian process with rapidly varying power along range. Additionally, a fast-moving target of interest has a few range cells migration within the coherent processing interval. Two coherent CFAR detectors are proposed taking into account target migration and highly inhomogeneous clutter. Both detectors involve solution of a transcendental equation, carried out numerically in a few iterations. The performance evaluation is addressed by numerical simulations and it shows a significant improvement in detection of fast-moving targets in inhomogeneous heavy tailed radar clutter.

Manuscript received July 5, 2016; revised January 16, 2017; released for publication June 1, 2017. Date of publication July 24, 2017; date of current version February 7, 2018.

DOI. No. 10.1109/TAES.2017.2731558

Refereeing of this contribution was handled by F. Gini.

This work was supported by Dutch Technology Foundation (STW) under Grant 12219.

Authors' addresses: N. Petrov, F. Le Chevalier, and A. G. Yarovoy are with the Microwave Sensing, Signals and Systems (MS3) Group, Delft Technical University, Delft 2628, The Netherlands, E-mail: (f.lechevalier@tudelft.nl; a.yarovoy@tudelft.nl; n.petrov@tudelft.nl). *(Corresponding author: Nikita Petrov.)*

I. INTRODUCTION

A new generation of modern radars tends to increase range resolution capabilities for better target detection and classification. Surveillance radars are especially interested in detection of moving targets—the situation, where the advantages of radars, being the sensors capable to distinguish between stationary and moving targets, are essential.

The time on target in modern surveillance radars is typically limited due to the need of scanning a large volume of space with a finite update time of the system. This implies a short time interval available for detection in every angular sector, subject to range-velocity ambiguity removal. The classical solution involves a combination of detection in a few bursts with different pulse repetition intervals (PRI) T_r in order to resolve ambiguities, resulting in a short coherent processing interval (CPI) in each burst (4–16 T_r) [1]. The reduction of CPI, given other waveform parameters fixed, leads to the following drawbacks: first, lower signal-to-clutter ratio (SCR) as a consequence of shorter integration time, which can be crucial for weak (e.g., stealth) target detection; second, the poor velocity resolution, which limits the capability of slow target detection.

On the other hand, long CPI can be used to improve target detection, but with a price of having ambiguities in narrow-band radars. Moreover, moving target observation in high-range resolution mode during relatively long CPI (say 50–100 ms) results in range migration phenomenon. This effect is well studied for target feature extraction (e.g., [2], [3]) and it can be efficiently compensated via Keystone [4] or Radon [5] transform. Such range-walk compensation allows to transform Doppler ambiguities present in low pulse repetition frequency (PRF) mode into the residual ambiguous sidelobes of the targets. The level of these ambiguous sidelobes is typically 6–20 dB, depending on the time-bandwidth product of transmitted pulse train [6], [7]. High-resolution spectrum techniques applied to such data benefit from range migration effect resulting in the ability to estimate the range-velocity map in low PRF mode unambiguously [7]–[9]. For weak targets of interest, a simple compensation of the range-walk can be sufficient to remove velocity ambiguities. In other words, for weak targets of interest, we consider the ambiguous sidelobes to be below the clutter or noise level and not generate additional false alarms.

Wideband surveillance radars benefit from the improvement in range resolution, which results in SCR gain, at least up to meter range resolution, when each target of interest (aircraft, car, etc.) can be considered as a point scatterer. Further improvement in range resolution allows to model each target as a set of point scatterers in a few adjacent range cells [10], [11]. The detection in this case can be considered as a generalization of a point target detector, while detection of a point target depends mostly on the clutter model used [12], [13].

An increase in range resolution affects clutter characteristics as well. The Gaussian model of clutter, used in narrow-band radars, is found not applicable in the

case of high-range resolution, see e.g., [13]–[17]. The modern trend is to model high-resolution radar clutter as a compound-Gaussian process (which belongs to the class of spherically invariant random vectors [13], [18], [19]) i.e., a Gaussian process with power varying from one range cell to another, but sharing the same correlation structure in slow time [13], [20]. This representation provides a mathematical tractable tool for clutter representation and further derivation of detection algorithms.

Constant false alarm rate (CFAR) target detection in compound-Gaussian clutter attracted significant attention during the last decades. A number of studies have been carried out on point (unresolved) target detection in non-Gaussian clutter, assuming both known [21], [22] and unknown [23], [24] probability density function (PDF) of the clutter. The latter exploits very important feature of being CFAR with respect to clutter power, which is of major importance for radar applications. Moreover, for long CPI the distribution-free test has been shown to approach the performance of the optimal one, as shown in [23] and [21]. The recent studies [18], [25]–[27] are focused on implementation of adaptive CFAR detector in compound-Gaussian clutter, which exploits the estimated covariance matrix (CM) of clutter. The discussion there is focused on strategies for CM estimation from the reference cells in spiky clutter and on the threshold setting for the adaptive detector. Also some studies investigate the detection of range-extended targets in compound-Gaussian clutter, e.g., [12] and [28]. A comprehensive overview of detection structures for modern radars can be found in [13]. However, target migration is typically not accounted for the detection, except of a few papers considering locally Gaussian clutter along the target range walk [29], [30].

Consequently, the main objective of this paper is to derive a CFAR detector for the case of range-migrating point target embedded in highly heterogeneous clutter following the compound-Gaussian model and to evaluate the benefits of applying CFAR detectors to migrating targets.

This paper is organized as follows. In Section II we recall the models of clutter and moving target observed by a wideband radar and exploit them to formulate the detection problem. Then, in Section III, two detectors utilizing different interpretations of compound-Gaussian clutter model are derived. The performance of the proposed techniques is studied via numerical simulations and presented in Section IV. Finally, the conclusions are given in Section V.

NOTATIONS Hereinafter, we use lowercase boldface letters for vector and uppercase boldface letters for matrices. Superscripts $(\cdot)^T$ and $(\cdot)^H$ stands for matrix/vector transpose and Hermitian transpose, respectively. We use notation $|\cdot|$ for matrix determinant, vec$(\cdot)$ for matrix vectorization, and tr$(\cdot)$ for the trace of a matrix. Also, in the following, we use the Heaviside step function – $\mathbb{1}(\cdot)$, the Dirac delta function – $\delta(\cdot)$, the Gamma function – $\Gamma(\cdot)$ and the modified Bessel function of the second kind of an order ν – $K_\nu(\cdot)$.

II. SIGNAL MODEL

To provide a mathematical formulation of the detection problem, the corresponding models of a migrating target and clutter observed by a wideband radar are revised in this section.

A. Target Model

The model of a migrating point target can be given considering K adjacent range cells including the target signature during the whole CPI. The signature of a moving target observed by a wideband radar is commonly expressed after applying fast Fourier transform on fast-time, thus in fast-frequency/slow-time domain, where it can be written as a bidimensional complex sinusoid with the coupling term modeling range migration [1], [7], [8]. With that said, the target signature in fast-frequency/slow-time is given by $K \times M$ matrix $\mathbf{T}^{\text{ft}}$ defined element-wise:

$$\mathbf{T}^{\text{ft}}_{n,m} = \exp\left(j2\pi\left(-\frac{\tau_0 B}{K}n + \frac{2v_0 f_c}{c}T_r\left(1+\frac{B}{Kf_c}n\right)m\right)\right). \tag{1}$$

Here $m = 0 \ldots M-1$ is the pulse (sweep) number, $n = 0 \ldots K-1$ is the fast-frequency index, T_r is PRI, f_c is the carrier frequency, and B is the waveform bandwidth, so the signal occupies frequencies from f_c to $f_c + B$. The point target has an initial time delay $\tau_0 = 2R_0/c$ depending on the initial target range (R_0), and constant velocity (v_0). The last term in (1) is specific for the wideband waveform, it models the range migration of the moving target and depends only on its radial velocity v_0. The superscript of $\mathbf{T}$ indicates the domain where the signal is described: "ft" stands to fast-frequency/slow-time, "tt" conforms for fast-time/slow-time domain.

The same target signature can be expressed in slow-time/fast-time [7]:

$$\mathbf{T}^{\text{tt}}_{k,m} = \exp\left(j2\pi\frac{2v_0 f_c}{c}T_r m\right) u_p\left(k-\left(k_0-\frac{v_0 T_r}{\delta_R}m\right)\right) \tag{2}$$

where $\mathbf{T}^{\text{tt}}$ is again $K \times M$ matrix, $k = 0 \ldots K-1$ is fast-time (range) index, k_0 stands for the initial range cell of the target, $\delta_R = c/(2B)$ is the radar range resolution, and $u_p(x)$ denotes the normalized pulse response of the transmitted waveform. Note that if the migration term $(v_0 T_r m/\delta_R)$ tends to zero, the signature of the target is present only in k_0th range cell and it folds into the one-dimensional sinusoid along slow time with the narrowband Doppler frequency. Hereinafter, we assume a waveform with a flat spectrum over the band, so $u_p(x) = \text{sinc}(\pi x)$.

Amplitude estimation of a range-velocity map can be obtained by coherent summation of the target signature in several adjacent range cells [1], [7]. Due to migration effect, the matched filter should be applied to the low-range resolution segment (LRRS) containing K range cells, such that the condition on maximal target velocity ($V_{\max}$) holds:

$$K \geq [V_{\max} M T_r/\delta_R] + \Delta_E \tag{3}$$

where $[x]$ stands for the rounding toward integer operation and Δ_E defines the extent of the target in range cells. In this paper, the problem of extended target detection is not considered, thus $\Delta_E = 1$.

Consequently, coherent detection of migrating target should be also performed on the LRRS of K range cells. Similar to the narrow-band case, the detection will be performed in fast-time/slow-time domain, so hereinafter we refer to (2) as a target signature and use $\mathbf{a} = \mathrm{vec}((\mathbf{T}^{\mathrm{tt}})^T)$ for its vectorized form.

B. Clutter Model

As discussed in the Introduction, the clutter response in each range cell k is modeled as a compound-Gaussian random vector, i.e., a product of two independent variables [20]:

$$\mathbf{c_k} = \sqrt{\tau_k}\mathbf{g_k} \tag{4}$$

where $M \times 1$ vector $\mathbf{c_k} = [c_{kM} \dots c_{(k+1)M-1}]^T$ represents the clutter response in the kth range cell. The clutter response in the whole LRRS is given by: $\mathbf{c} = [\mathbf{c_0}^T, \mathbf{c_1}^T, \dots, \mathbf{c_{K-1}}^T]^T$. The speckle component in the kth range cell $\mathbf{g_k}$ is modeled as complex multivariate Gaussian M-vector with zero mean and CM $E(\mathbf{g_k}\mathbf{g_k}^H) = \mathbf{M_v}$, i.e., $\mathbf{g_k} \sim CN(\mathbf{0}, \mathbf{M_v})$; and τ_k is the texture parameter in the kth range cell. Therefore, in each range cell clutter CM is given by $E\{\mathbf{c_k}\mathbf{c_k}^H\} = E_{\mathrm{T}}\{\tau_k\}\mathbf{M_v}$. Subscript E_{T} states that expectation can be taken only over slow time, not over range.

Two models of the texture parameters τ_k have been proposed so far: independent interference model, where the textures $\tau_k, k = 0 \dots K-1$ are independent and identically distributed (IID) random variables; and dependent interference model, where the parameters τ_k of clutter are correlated over range [16]. The independent interference model has been used to derive normalized matched filter (NMF) [23], it was also exploited to infer the methods for CM structure estimation, e.g., [25]. The analysis of real data records in [16] shows its good fitness for the case when the reference cells are taken away from the cell under test (CUT) and in general for statistical analysis of high-resolution radar clutter [15]. The results in [17] show that this model fits well in the case of grass vegetation ground clutter, but it is less suitable for the scene with trees and forest. The dependent interference model results in the correlation of texture parameters τ_k over range. Different models of range correlation of texture were studied in [17] and [20], resulting in the conclusion that correlation behavior is dependent on many factors: polarization, grazing angle, wind speed, etc., and can be retrieved form the data. The compromise between the aforementioned two models can be obtained by clustering the clutter responses into groups of a few range cells sharing the same local power, but varying from group to group [12]. The length of the cluster can be evaluated from the average correlation interval over range, *a priori*.

Having defined the model of a range migrating target, we should clarify the impact of range migration effect on clutter. Phenomenologically, clutter can be interpreted as a reflection from nearly stationary objects, which are out of interest for moving target detection. Therefore, the migration term in the model (2) can be ignored for the clutter scatterers. This assumption is used to distinguish between clutter and targets in [6].

Moreover, the clutter texture in a range cell can slowly vary in time, which is essentially important for modeling sea clutter during moderate observation time. However, for ground clutter or short CPI employed for moving target detection, this effect can be neglected, resulting in constant τ_k over the whole CPI. The latter model is commonly referred as completely correlated texture, and used to derive most detectors in compound-Gaussian clutter [21].

In this paper, we focus on the independent interference model with completely correlated texture, which is considered as a tradeoff between fitting high-resolution real data and complexity of the model. In particular, it does not require knowledge of the texture correlation along range and slow-time, which can be difficult to estimate in real scenarios (e.g., urban areas). Independent interference model satisfies $E\{\mathbf{c_k}\mathbf{c_i}^H\}|_{k\neq i} = \mathbf{0}$ and, as the result, the clutter CM in an LRRS has the block-diagonal structure:

$$\mathbf{M} = \begin{bmatrix} E_{\mathrm{T}}\{\tau_0\}\mathbf{M_v} & \mathbf{0} & \cdots & \mathbf{0} \\ \mathbf{0} & E_{\mathrm{T}}\{\tau_1\}\mathbf{M_v} & \cdots & \mathbf{0} \\ \vdots & \vdots & \ddots & \vdots \\ \mathbf{0} & \mathbf{0} & \cdots & E_{\mathrm{T}}\{\tau_{K-1}\}\mathbf{M_v} \end{bmatrix}. \tag{5}$$

C. Problem Formulation

The detection problem consists of testing the hypothesis of target presence H_1 against the clutter only hypothesis H_0:

$$\mathbf{y} = \begin{cases} H_0: & \mathbf{c_k} \\ H_1: & \alpha\mathbf{a_k} + \mathbf{c_k} \end{cases} \qquad k = 0 \dots K-1 \tag{6}$$

where $\mathbf{y} = [\mathbf{y_0}^T, \mathbf{y_1}^T, \dots, \mathbf{y_{K-1}}^T]^T$ is the received data in the LRRS under test containing range cells $k = 0 \dots K-1$. In every kth range cell, the received data $\mathbf{y_k} = [\mathbf{y}_{kM}, \dots, \mathbf{y}_{(k+1)M-1}]^T$ includes an independent response of clutter $\mathbf{c_k}$ and possibly the target with the known steering vector $\mathbf{a_k} = [\mathbf{a}_{kM}, \dots, \mathbf{a}_{(k+1)M-1}]^T$ in this range cell, but unknown complex amplitude α, constant within CPI.

In order to obtain CFAR detector, we perform the generalized likelihood ratio test (GLRT) [31]. The nearest problem to the one we try to solve is the detection of a nonmigrating point target in non-Gaussian clutter. As previously stated, there are two competing models of the clutter involved in the derivations of a coherent radar detector for such interference. For radar applications, it is more common to model clutter with compound-Gaussian model, where the texture is a random variable with some PDF. This approach is used, e.g., in [23], to derive NMF with assumption that the structure of clutter CM $\mathbf{M_v}$ is known. The second approach considers a realization of the texture in the range CUT as an additional unknown

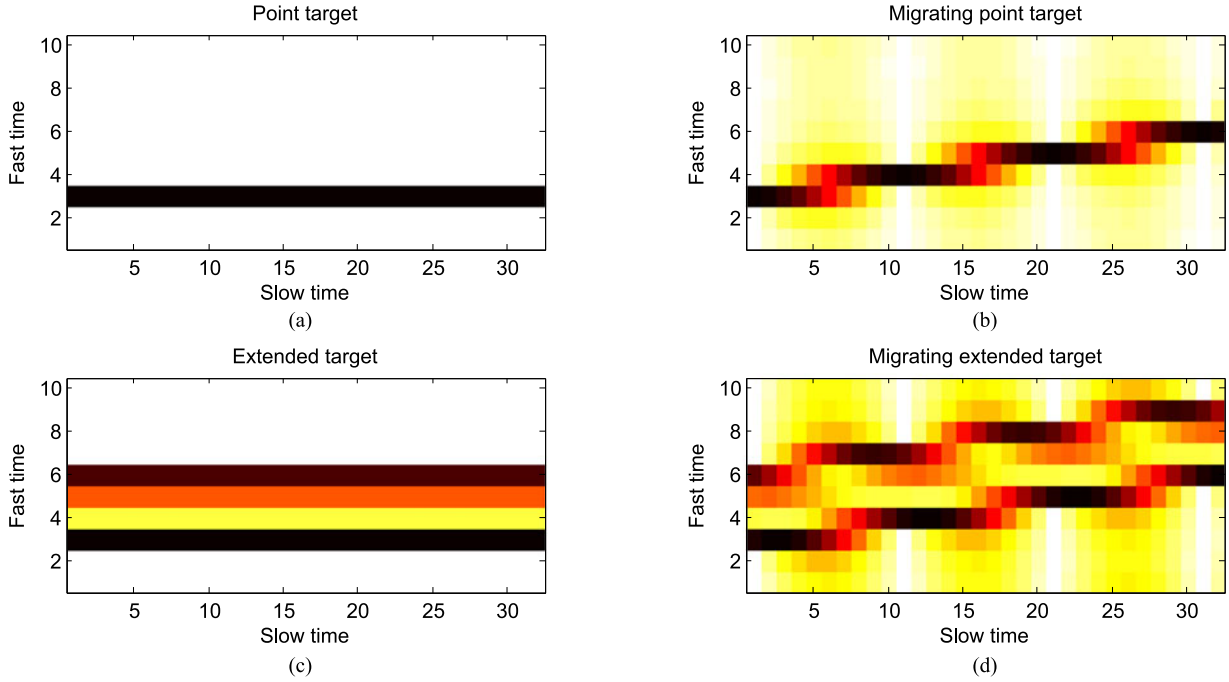

Fig. 1. Target signature of: (a) a point nonmigrating target; (b) a point migrating target; (c) an extended nonmigrating target; (d) an extended migrating target.

deterministic parameter (instead of a random variable). In fact, this is tantamount considering Gaussian clutter with unknown power in each range cell, but constant within CPI. As a result, the latter approach leads to the same detection structure as previously, thus NMF [24], [32]. The approximation used to derive NMF under compound-Gaussian model is fair only for large number of pulses in CPI, for small M known clutter PDF results in performance gain [21]. For a nonmigrating target detection, NMF is applied to a single range cell, say k_0, and it is given by

$$\frac{|\mathbf{a_{k_0}}^H \mathbf{M_v^{-1}} \mathbf{y_{k_0}}|^2}{\left(\mathbf{a_{k_0}^H M_v^{-1} a_{k_0}}\right)\left(\mathbf{y_{k_0}^H M_v^{-1} y_{k_0}}\right)} \underset{H_0}{\overset{H_1}{\gtrless}} T_{\mathrm{NB-NMF}} \tag{7}$$

where $\mathbf{a_{k_0}} = [\mathbf{a}_{k_0 M}, \ldots, \mathbf{a}_{(k_0+1)M-1}]^T$ is the narrow-band (without migration) steering vector in the range cell k_0, derived from (2) assuming $|v_0| T_r M/\delta_R \ll 1$. This model is shown in Fig. 1(a).

In case of range-extended target with no migration, the adjacent range cells of the target response are considered to be independent from each other. Moreover, due to the absence of range-walk, the scatterers are assumed to be present in the same range cells during the whole CPI, as shown in Fig. 1(c). The decision rule then becomes a combination of the statistics (7) estimated from the range cells on the target [13], [28].

On the other hand, fast-moving targets do not satisfy the requirement on the scatterer presence in one range cell during the whole CPI, so the migration should be considered for detection as shown in Fig. 1(b). So far, detection of range migrating targets has been considered in locally Gaussian environment only [29], [30], assuming $\tau_0 = \ldots = \tau_{K-1} = \tau$. In this case, the detection is performed by NMF with the correct (taking into account range migration) target signature $\mathbf{a}$ applied to the whole LRRS directly:

$$\frac{|\mathbf{a}^H \mathbf{M^{-1}} \mathbf{y}|^2}{\left(\mathbf{a}^H \mathbf{M^{-1}} \mathbf{a}\right)\left(\mathbf{y}^H \mathbf{M^{-1}} \mathbf{y}\right)} \underset{H_0}{\overset{H_1}{\gtrless}} T_{\mathrm{LRR-NMF}}. \tag{8}$$

However, if the locally Gaussian assumption is not valid, because of rapidly varying texture along range, this test is not CFAR anymore. Moreover, real fast-moving targets, observed by a wideband radar, are both extended and range migrating, as shown in Fig. 1(d). However, the detection of extended target is not considered in this study, so we focus on the model shown in Fig. 1(b). Finally, in practical applications, the aforementioned detectors exploit CM estimated from the reference cells, resulting in the appropriate change of the threshold [18], [26].

Coming back to the problem of migrating target detection in a highly inhomogeneous clutter, the GLRT for the compound-Gaussian model can be written in the following form:

$$\Lambda(\mathbf{Z}, \mathbf{y}) = \frac{\max_{\tau_{\mathcal{K}}, \tau_{\mathcal{L}}, \mathbf{M_v}, \alpha} f_1(\mathbf{y}, \mathbf{Z}; \alpha, \tau_{\mathcal{K}}, \tau_{\mathcal{L}}, \mathbf{M_v})}{\max_{\tau_{\mathcal{K}}, \tau_{\mathcal{L}}, \mathbf{M_v}} f_0(\mathbf{y}, \mathbf{Z}; \tau_{\mathcal{K}}, \tau_{\mathcal{L}}, \mathbf{M_v})} \underset{H_0}{\overset{H_1}{\gtrless}} T \tag{9}$$

where $f_0(\mathbf{y}, \mathbf{Z}; \tau_{\mathcal{K}}, \tau_{\mathcal{L}}, \mathbf{M_v})$ stands for the joint PDF of LRRS and the reference cells under H_0 and its counterpart under H_1 is $f_1(\mathbf{y}, \mathbf{Z}; \alpha, \tau_{\mathcal{K}}, \tau_{\mathcal{L}}, \mathbf{M_v})$. The matrix $\mathbf{Z}$ of size $M \times L$ contains M-dimensional data from the reference range cells $\mathbf{z}_{\mathcal{L}}$, $\mathcal{L} : l = 0 \ldots L-1$ as columns, where L is the number of reference cells for estimation of $\mathbf{M_v}$. The unknown parameters involved in both PDFs are the texture in the LRRS under test $\tau_{\mathcal{K}}$, where $\mathcal{K} : k = 0 \ldots K-1$, the

texture in the reference cells $\tau_{\mathcal{L}}$, the structure of clutter CM in slow time $\mathbf{M_v}$, and the amplitude of the target α under hypothesis H_1. Note that in general clutter texture τ is a random variable defined by its PDF, but the particular realizations $\tau_{\mathcal{K}}$, $\tau_{\mathcal{L}}$ are unknowns, because they are random quantities.

In order to proceed further, we assume that the structure of clutter CM in one range cell, i.e., $\mathbf{M_v}$, is known and we look for a detector capable to deal with range migrating targets. This simplification allows us to remove $\tau_{\mathcal{L}}$, $\mathbf{Z}$, and $\mathbf{M_v}$ from the GLRT (9). The proposed detection algorithms are presented in Section III.

III. MIGRATING TARGET DETECTOR

In this section, we focus on a design of CFAR detector for a range migrating target in compound-Gaussian clutter using aforementioned simplification of the GLRT. Two strategies are studied: first, we consider a compound-Gaussian model, where the texture τ is a random variable with known PDF. Second, we perform a suboptimal approach by considering texture as an unknown parameter in GLRT, and substitute its estimation into the test. In fact, the second approach considers compound-Gaussian clutter as being Gaussian with unknown power in each range cell and leads to a distribution-free test, which is of practical interest.

A. Texture is a Realization of Random Variable With Known PDF

The independent interference model considered in this study allows us to represent the PDF of the data in the absence of a target (H_0) in each range cell separately. The clutter, being compound-Gaussian, satisfies the following PDF in every range cell [20], [33], assuming $\mathbf{M_v}$ is known and satisfies $\mathrm{tr}(\mathbf{M_v}) = M$:

$$f_0(\mathbf{y_k}) = E\{f_0(\mathbf{y_k}|\tau_k)\} = \int_0^\infty \frac{1}{(\pi\tau_k)^M |\mathbf{M_v}|} \exp\left(-\frac{\mathbf{y_k}^H \mathbf{M_v^{-1}} \mathbf{y_k}}{\tau_k}\right) p_\tau(\tau_k)\, d\tau_k \quad (10)$$

where $p_\tau(\tau_k)$ is the known PDF of clutter texture in kth range cell of the LRRS under test. Due to independent interference model used, the PDF of the whole LRRS under H_0 can be given as a product of the PDFs over K range cells:

$$f_0(\mathbf{y}) = \prod_{k=0}^{K-1} \int_0^\infty \frac{\exp\left(-\tau_k^{-1} \mathbf{y_k}^H \mathbf{M_v^{-1}} \mathbf{y_k}\right)}{(\pi\tau_k)^M |\mathbf{M_v}|} p_\tau(\tau_k)\, d\tau_k. \quad (11)$$

Under hypothesis H_1, the PDF of the LRRS under test is derived from the PDF under H_0 by setting the mean value of the Gaussian form to be equal to the present signal $\mathbf{s} = \alpha\mathbf{a}$, where $\mathbf{a}$ is known steering vector and α is unknown, but constant withing CPI complex amplitude of the target. The PDF of the LRRS under hypothesis of target presence (H_1) is then written using the known steering vector of the target in the kth range cell $\mathbf{a_k}$ as

$$f_1(\mathbf{y};\alpha) = \prod_{k=0}^{K-1} \int_0^\infty p_\tau(\tau_k) \cdot \frac{\exp\left(-\tau_k^{-1}(\mathbf{y_k} - \alpha\mathbf{a_k})^H \mathbf{M_v^{-1}} (\mathbf{y_k} - \alpha\mathbf{a_k})\right)}{(\pi\tau_k)^M |\mathbf{M_v}|} d\tau_k. \quad (12)$$

The PDFs under both hypotheses being defined, the GLRT (9) reduces to the test:

$$\Lambda(\mathbf{y}) = \frac{f_1(\mathbf{y};\alpha)}{f_0(\mathbf{y})} \underset{H_0}{\overset{H_1}{\gtrless}} T \quad (13)$$

where the dependence on the texture within LRRS $\tau_{\mathcal{K}}$ is removed assuming its PDF is known. On the other hand, no prior information about α is available, thus it should be substituted with its maximum likelihood estimation (MLE).

Furthermore, we assume the clutter to be IID (hence compound-Gaussian), which implies equal distribution of texture along range: $p_\tau(\tau_0) = \ldots = p_\tau(\tau_k) = \ldots = p_\tau(\tau_{K-1}) = p_\tau(\tau)$. This fact allows us to simplify the PDFs under both hypotheses (11), (12) by means of the following function [16], [25]:

$$h_M(x) = \int_0^\infty \tau^{-M} \exp\left(-\frac{x}{\tau}\right) p_\tau(\tau)\, d\tau \quad (14)$$

resulting in the following expression for PDF of the LRRS under H_1:

$$f_1(\mathbf{y};\alpha) = \frac{\prod_{k=0}^{K-1} h_M\left((\mathbf{y_k} - \alpha\mathbf{a_k})^H \mathbf{M_v^{-1}} (\mathbf{y_k} - \alpha\mathbf{a_k})\right)}{|\mathbf{M_v}|^K \pi^{KM}}. \quad (15)$$

As usually, the PDF under H_0 is: $f_0(\mathbf{y}) = f_1(\mathbf{y};\alpha)|_{\alpha=0}$. The PDF of texture is included in the function h_M.

Next, the PDF under H_1 should be maximized over the unknown deterministic target amplitude α. Instead of maximization of the likelihood function, its logarithm can be maximized by taking the derivative and setting it to zero. It is done using the relation for derivative of function $h_M(x)$: $\partial h_M(x)/\partial x = -h_{M+1}(x)$ and constructing the function $c_M(x) = h_{M+1}(x)/h_M(x)$. Finally, the amplitude estimation has the form:

$$\hat{\alpha} = \frac{\sum_{k=0}^{K-1} c_M\left((\mathbf{y_k} - \hat{\alpha}\mathbf{a_k})^H \mathbf{M_v^{-1}} (\mathbf{y_k} - \hat{\alpha}\mathbf{a_k})\right) \mathbf{a_k}^H \mathbf{M_v^{-1}} \mathbf{y_k}}{\sum_{k=0}^{K-1} c_M\left((\mathbf{y_k} - \hat{\alpha}\mathbf{a_k})^H \mathbf{M_v^{-1}} (\mathbf{y_k} - \hat{\alpha}\mathbf{a_k})\right) \mathbf{a_k}^H \mathbf{M_v^{-1}} \mathbf{a_k}}. \quad (16)$$

Therefore, in order to find $\hat{\alpha}$, we have to solve the transcendental equation (16), which can be solved iteratively, subject to known PDF of the clutter texture $p_\tau(\tau)$. The derived estimation of $\hat{\alpha}$ should be substituted into GLRT

$$\hat{\Lambda}(\mathbf{y}) = \prod_{k=0}^{K-1} \frac{h_M\left((\mathbf{y_k} - \hat{\alpha}\mathbf{a_k})^H \mathbf{M_v^{-1}} (\mathbf{y_k} - \hat{\alpha}\mathbf{a_k})\right)}{h_M\left(\mathbf{y_k}^H \mathbf{M_v^{-1}} \mathbf{y_k}\right)} \underset{H_0}{\overset{H_1}{\gtrless}} T \quad (17)$$

in order to perform detection.

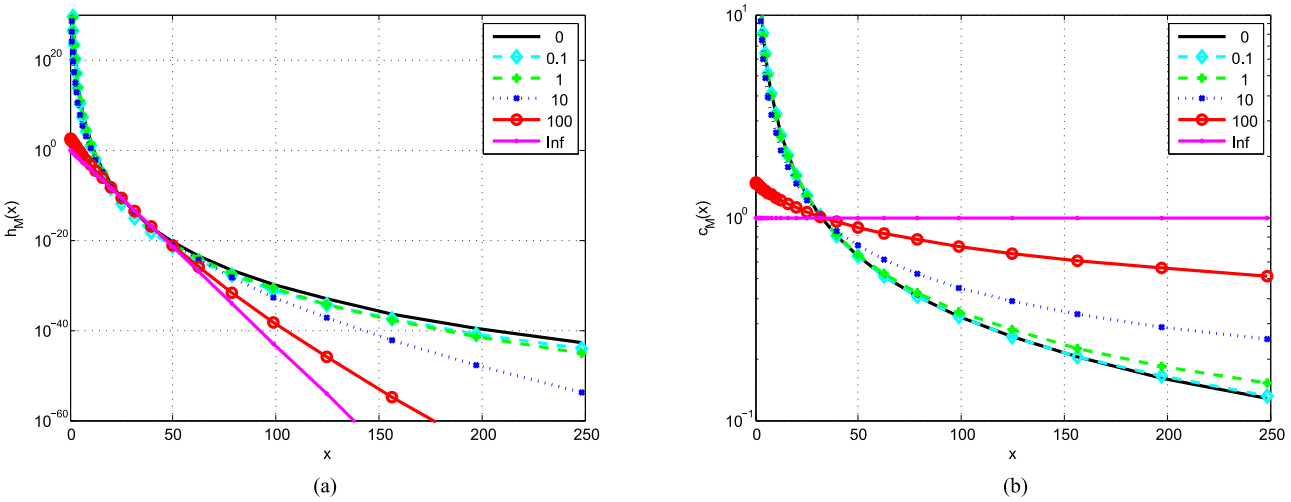

Fig. 2. Weighting coefficients for different values of clutter shape ν, $M = 32$: (a) $h_M(x)$, (b) $c_M(x)$.

Note that the functions $c_M(x)$ and $h_M(x)$ are identical to the ones used for clutter CM structure estimation in compound-Gaussian clutter, when the distribution of texture is known [25]. For practical application this means that estimation of $\mathbf{M_v}$ and detection can be done on the same (or identical) chain.

A particular case of compound Gaussian distribution is K-distribution, used to describe high-resolution radar clutter [14], [17], [20]. In this case, the texture parameter follows Gamma distribution:

$$p_\tau(\tau) = \frac{1}{\Gamma(\nu)}\left(\frac{\nu}{\mu}\right)^{\nu}\tau^{\nu-1}\exp\left(-\frac{\nu}{\mu}\tau\right)\mathbb{1}(\tau) \tag{18}$$

where μ and ν are the scale and shape parameters of Gamma distribution, respectively. Then, the joint PDF of the LRRS can be expressed by substitution (18) into (14) and (15) and nonlinear functions $h_M(x)$ and $c_M(x)$ can be written analytically:

$$\begin{aligned} h_M(x) &= \frac{2x^{\frac{\nu-M}{2}}}{\Gamma(\nu)}\left(\frac{\nu}{\mu}\right)^{\frac{\nu+M}{2}} K_{\nu-M}\left(\sqrt{4\nu x/\mu}\right); \\ c_M(x) &= \sqrt{\frac{\nu}{\mu x}}\frac{K_{\nu-M-1}\left(\sqrt{4\nu x/\mu}\right)}{K_{\nu-M}\left(\sqrt{4\nu x/\mu}\right)}. \end{aligned} \tag{19}$$

The plots of these functions involved in (16) and (17) are shown in Fig. 2 for $M = 32$ and $\mu = 1$.

It is interesting to consider two extreme cases of K-distribution shape parameter, i.e., $\nu \to 0$ and $\nu \to \infty$. If $\nu \to \infty$, then the clutter tends to Gaussian distribution with power $p_\tau(\tau) = \delta(\tau - \mu)$, where μ is the known mean power of clutter. By definition (14), the nonlinear memoryless function $h_M(x)$ reduces to $h_M^\infty(x) = \mu^{-M}\exp(-x/\mu)$, which is linear in a logarithmic scale, and, accordingly, $c_M(x)$ degenerates to a constant: $c_M^\infty(x) = \mu^{-1}$ (superscript of functions h_M and c_M stands for specific value of K distribution shape parameter ν). As it can be expected, in this case, MLE of $\hat{\alpha}$ simplifies to its form in Gaussian interference:

$$\hat{\alpha} = \frac{\sum_{k=0}^{K-1}\mathbf{a_k}^H\mathbf{M_v^{-1}}\mathbf{y_k}}{\sum_{k=0}^{K-1}\mathbf{a_k}^H\mathbf{M_v^{-1}}\mathbf{a_k}} = \frac{\mathbf{a}^H\mathbf{M^{-1}}\mathbf{y}}{\mathbf{a}^H\mathbf{M^{-1}}\mathbf{a}} \tag{20}$$

where the second equality is obtained using the model of the CM of clutter in LRRS (5) with equal values of texture parameter $E\{\tau_k\} = \mu$, $\forall k \in \mathcal{K}$. Straightforward simplification of the GLRT (17) by means of (20) leads to the following expression of the logarithm of GLRT:

$$\ln\left(\hat{\Lambda}(y)\right) = \frac{\left|\mathbf{a}^H\mathbf{M^{-1}}\mathbf{y}\right|^2}{\mu\,\mathbf{a^H M^{-1}}\mathbf{a}} \tag{21}$$

which is a general form of a scale-invariant detector used in [32]. The particular case of clutter scale parameter $\mu = 1$ then degenerates to the matched filter detector [31].

The other limiting case appears when $\nu \to 0$. Gamma PDF is not defined for $\nu \to 0$, but we expect to have an effect just opposite to the previous case, thus the PDF of the texture should have some noninformative prior. For example, it can be assumed flat over all possible values of τ bounded above by $\tau_{\max}$: $p_\tau(\tau) = (\mathbb{1}(0) - \mathbb{1}(\tau_{\max}))/\tau_{\max}$, and now the upper limit of the integral in (14) is $\tau_{\max}$. The integral (14) then can be solved by letting $\tau_{\max} \to +\infty$ and changing the variable $z = 1/\tau$ (see [34, 3.351.3]). The resulting nonlinear functions are $h_M^0(x) = \Gamma(M)\,x^{-M}$ and $c_M^0(x) = M/x$. In this case, amplitude estimation reduces to

$$\hat{\alpha} = \frac{\sum_{k=0}^{K-1}\frac{\mathbf{a}_k^H\mathbf{M_v^{-1}}\mathbf{y_k}}{(\mathbf{y_k}-\hat{\alpha}\mathbf{a_k})^H\mathbf{M_v^{-1}}(\mathbf{y_k}-\hat{\alpha}\mathbf{a_k})}}{\sum_{k=0}^{K-1}\frac{\mathbf{a}_k^H\mathbf{M_v^{-1}}\mathbf{a_k}}{(\mathbf{y_k}-\hat{\alpha}\mathbf{a_k})^H\mathbf{M_v^{-1}}(\mathbf{y_k}-\hat{\alpha}\mathbf{a_k})}} \tag{22}$$

and the GLRT (17) has a form:

$$\hat{\Lambda}(\mathbf{y}) = \prod_{k=1}^{K}\left(\frac{(\mathbf{y_k}-\hat{\alpha}\mathbf{a_k})^H\,\mathbf{M_v^{-1}}\,(\mathbf{y_k}-\hat{\alpha}\mathbf{a_k})}{\mathbf{y_k}^H\mathbf{M_v^{-1}}\mathbf{y_k}}\right)^{-M} \underset{H_0}{\overset{H_1}{\gtrless}} T. \tag{23}$$

Note that in case of any value of $\nu < +\infty$ (so, except of the Gaussian clutter), the estimation of $\hat{\alpha}$, required in the GLRT, is defined by the transcendental equation, and so it has to be solved iteratively. Two limiting cases $\nu \to 0$ and $\nu \to \infty$ with $\mu = 1$ are also shown in Fig. 2 for comparison.

B. Texture is an Unknown Parameter

In many cases no knowledge about clutter texture is available, so the test can be reformulated in terms of GLRT, considering the realization of texture in each range cell as an unknown parameter. Even though substitution of unknown parameter with its estimation typically leads to a suboptimal detection strategy, the resulting detectors are often practical due to their simple implementation. Considering clutter texture as being an unknown parameter degenerates compound-Gaussian clutter toward the Gaussian model with unknown power in each range cell [24]. For clarity, in this section, we denote local power of clutter (a realization of the texture) in the kth range with σ_k^2 (instead of τ_k).

As before, we assume clutter with completely correlated texture and known structure of CM in slow-time $\mathbf{M_v}$, but the target migrates within a few range cells including the clutter of different (unknown) powers $\sigma_{\mathcal{K}}^2$. Under H_1, the target is present in the LRRS under test with known signature $\mathbf{a}$, its complex amplitude α is constant within CPI, but unknown. Moreover, we consider independent interference model of clutter, which results in the following PDF of LRRS under H_1:

$$f_1(\mathbf{y}; \alpha, \sigma_{\mathcal{K}}^2) = \frac{\exp\left(-\sum_{k=1}^{K} \sigma_k^{-2} (\mathbf{y_k} - \alpha \mathbf{a_k})^H \mathbf{M_v^{-1}} (\mathbf{y_k} - \alpha \mathbf{a_k})\right)}{\pi^{KM} |\mathbf{M_v}|^K \prod_{k=1}^{K} \sigma_k^{2M}} \tag{24}$$

and the PDF of LRRS under H_0 is given by $f_0(\mathbf{y}; \sigma_{\mathcal{K}}^2) = f_1(\mathbf{y}; \alpha, \sigma_{\mathcal{K}}^2)|_{\alpha=0}$. Under H_0, the PDF of the LRRS $f_0(\mathbf{y}; \sigma_{\mathcal{K}}^2)$ involves unknown local powers in each range cell $\sigma_{\mathcal{K}}^2$. Under H_1, the PDF of LRRS in addition depends on the unknown target amplitude α. In these terms, the GLRT is given by

$$\Lambda(\mathbf{y}) = \frac{f_1(\mathbf{y}; \alpha, \sigma_{\mathcal{K}}^2)}{f_0(\mathbf{y}; \sigma_{\mathcal{K}}^2)} \underset{H_0}{\overset{H_1}{\gtrless}} T. \tag{25}$$

To derive a detector, all unknown parameters should be substituted by their MLEs. We start with MLE of local clutter power in each range cell σ_k^2 under both hypotheses. It can be obtained by maximizing the logarithm of the likelihood functions under both hypotheses. Then, the estimation of the local power of clutter in each range cell is given under H_1:

$$\hat{\sigma}_{1k}^2 = \frac{1}{M} (\mathbf{y_k} - \alpha \mathbf{a_k})^H \mathbf{M_v^{-1}} (\mathbf{y_k} - \alpha \mathbf{a_k}), \ \forall k \in \mathcal{K}. \tag{26}$$

Similarly under H_0: $\hat{\sigma}_{0k}^2 = \hat{\sigma}_{1k}^2|_{\alpha=0}$.

Using these values in the GLRT (25) it can be simplified to

$$\hat{\Lambda}(\mathbf{y}) = \left(\prod_{k=0}^{K-1} \frac{\hat{\sigma}_{0k}^2}{\hat{\sigma}_{1k}^2}\right)^M = \left(\prod_{k=0}^{K-1} \frac{\mathbf{y_k^H M_v^{-1} y_k}}{(\mathbf{y_k} - \alpha \mathbf{a_k})^H \mathbf{M_v^{-1}} (\mathbf{y_k} - \alpha \mathbf{a_k})}\right)^M \underset{H_0}{\overset{H_1}{\gtrless}} T. \tag{27}$$

In order to find α, we need to maximize the logarithm of (27), which can be done by taking the derivative and setting it to zero. Finally, the amplitude estimation $\hat{\alpha}$ is written by the transcendental equation in the form (22). Equivalent representation can be given using the local power of clutter under H_1 (26):

$$\hat{\alpha} = \frac{\sum_{k=0}^{K-1} \hat{\sigma}_{1k}^{-2} \mathbf{a_k^H M_v^{-1} y_k}}{\sum_{k=0}^{K-1} \hat{\sigma}_{1k}^{-2} \mathbf{a_k^H M_v^{-1} a_k}}. \tag{28}$$

The coincidence of the results (22) and (28) [using $\hat{\sigma}_{1k}^2$ from (26)] can be explained as follows. The derivations for random texture can be considered as a Bayesian Neyman–Pearson detector, for which the distribution of $\tau_{\mathcal{K}}$ is given, while α has a noninformative prior. Thus, if we assume $\tau_{\mathcal{K}}$ to have noninformative prior as well (see $\nu \to 0$ before), the detector (17) becomes equivalent to GLRT [31].

On the other hand, from (26) and (28), we can write the transcendental equation with respect to $\hat{\sigma}_{1k}^2$, $\forall k \in \mathcal{K}$:

$$\hat{\sigma}_{1k}^2 = \frac{1}{M} \left(\mathbf{y_k} - \frac{\sum_{i=0}^{K-1} \hat{\sigma}_{1i}^{-2} \mathbf{a_i^H M_v^{-1} y_i}}{\sum_{i=0}^{K-1} \hat{\sigma}_{1i}^{-2} \mathbf{a_i^H M_v^{-1} a_i}} \mathbf{a_k}\right)^H \mathbf{M_v^{-1}} \cdot \left(\mathbf{y_k} - \frac{\sum_{i=0}^{K-1} \hat{\sigma}_{1i}^{-2} \mathbf{a_i^H 0} M_v^{-1} y_i}{\sum_{i=0}^{K-1} \hat{\sigma}_{1i}^{-2} \mathbf{a_i^H M_v^{-1} a_i}} \mathbf{a_k}\right) \tag{29}$$

where the whole set of $\hat{\sigma}_{1\mathcal{K}}^2$ should be updated at each iteration. Both (22) and (29) have a form of a fixed point iteration and can be solved iteratively. The local convergence of the estimator (22) is proven in the Appendix.

Similarly to the approach in [25], the iterative procedure can be represented in two equations:

$$\begin{cases} \hat{\alpha} = \dfrac{\sum_{k=0}^{K-1} \hat{\sigma}_{1k}^{-2} \mathbf{a_k^H M_v^{-1} y_k}}{\sum_{k=0}^{K-1} \hat{\sigma}_{1k}^{-2} \mathbf{a_k^H M_v^{-1} a_k}}, \\ \hat{\sigma}_{1k}^2 = \dfrac{1}{M} (\mathbf{y_k} - \hat{\alpha} \mathbf{a_k})^H \mathbf{M_v^{-1}} (\mathbf{y_k} - \hat{\alpha} \mathbf{a_k}), \quad \forall k. \end{cases} \tag{30}$$

In this case, the system should be solved using two-step person-by-person alternate maximization (AM) algorithm, similar to CM estimation in compound-Gaussian clutter [25]. The iterative algorithm at each step assumes one unknown $\hat{\sigma}_{1\mathcal{K}}^2$ or $\hat{\alpha}$ to be fixed and calculates the MLE of the other. The output of the iterative procedure should be substituted into the GLRT (27).

C. False Alarm Regulation

The derivations presented above constrain target velocity only with a requirement of its physical presence in the

LRRS during the whole CPI. If this condition is satisfied, the detection structures presented above are independent on the target velocity. Therefore, in order to set the threshold, we can consider the particular case of nonmoving and, what is more important, nonmigrating target, i.e., $\upsilon_0 = 0$. The target, being a point scatterer, is thus present in one range cell, say k_i, $0 \le k_i \le K-1$. In the other range cells, the target signature is zero: $\mathbf{a_k} = \mathbf{0}_M, \forall k \ne k_i$. Consequently both tests (17), (27) reduce to their narrow-band counterparts and amplitude estimation can be obtained directly: $\hat{\alpha} = \mathbf{a}_{\mathbf{k_i}}^H \mathbf{M_v^{-1}} \mathbf{y}_{\mathbf{k_i}} / \mathbf{a}_{\mathbf{k_i}}^H \mathbf{M_v^{-1}} \mathbf{a}_{\mathbf{k_i}}$. As a result, the test (17) has a form:

$$\Lambda(\mathbf{y}) = \frac{h_M\left(\mathbf{y}_{\mathbf{k_i}}^H \mathbf{M_v^{-1}} \mathbf{y}_{\mathbf{k_i}} - \frac{|\mathbf{a}_{\mathbf{k_i}}^{\mathbf{H}} \mathbf{M_v^{-1}} \mathbf{y}_{\mathbf{k_i}}|^2}{\mathbf{a}_{\mathbf{k_i}}^{\mathbf{H}} \mathbf{M_v^{-1}} \mathbf{a}_{\mathbf{k_i}}}\right)}{h_M\left(\mathbf{y}_{\mathbf{k_i}}^H \mathbf{M_v^{-1}} \mathbf{y}_{\mathbf{k_i}}\right)} \underset{H_0}{\overset{H_1}{\gtrless}} T. \tag{31}$$

For well-behaved $p_\tau(\tau)$ and large M, which is considered herein, GLRT (31) can be replaced with

$$\Lambda(\mathbf{y}) = \left(\frac{1}{1-\gamma}\right)^M = (1-\gamma)^{-M} \tag{32}$$

where $\gamma = \left|\mathbf{a}_{\mathbf{k_i}}^H \mathbf{M_v^{-1}} \mathbf{y}_{\mathbf{k_i}}\right|^2 / \left(\mathbf{y}_{\mathbf{k_i}}^H \mathbf{M_v^{-1}} \mathbf{y}_{\mathbf{k_i}} \mathbf{a}_{\mathbf{k_i}}^H \mathbf{M_v^{-1}} \mathbf{a}_{\mathbf{k_i}}\right)$ [16], [35]. Note that GLRT in case of texture considered as an unknown parameter (27) reduces to the same test. Under H_0 variable γ follows beta distribution with parameters $\gamma_0 \sim \beta(1, M-1)$, for detection γ has to be compared with $T_\gamma = 1 - P_{FA}^{1/(M-1)}$ [16], [23].

Unfortunately, γ is not defined in the presence of target migration, when only iterative estimation of amplitude is available. In order to proceed further, we can use the likelihood ratio transformed via monotonic function $\psi(x) = x^{-1/M}$. Under H_0, the PDF of transformed likelihood ratio can be derived using the mirror-image symmetry of beta distribution:

$$(\Lambda_0(\mathbf{y}))^{-\frac{1}{M}} = (1-\gamma_0) \sim \beta(M-1, 1). \tag{33}$$

Note that because of using monotonically decreasing function $\psi(x)$ the inequality sign for comparison $(\Lambda(\mathbf{y}))^{-\frac{1}{M}}$ with the threshold should be changed. Obviously, the statistics $\Lambda(\mathbf{y})$ is now defined for any velocity, independently on target migration, and the decision rule for $\Lambda(\mathbf{y})$ can be written:

$$\Lambda(\mathbf{y}) \underset{H_0}{\overset{H_1}{\lessgtr}} P_{FA}^{-\frac{M}{M-1}}. \tag{34}$$

Note that the threshold for both detectors is independent on users parameter K—the number of range cells in the LRRS. The only restriction is that the target should be present in the LRRS under test during the whole CPI.

Implementation of an adaptive detector will require to adjust the threshold according to the CM estimation employed in the detector. However, adaptive detection in structured interference with block-diagonal CM (5) was shown to be a challenging task [30], [36]. Therefore, we leave the problem of threshold setting for an adaptive detection for the future research.

TABLE I
Parameters of Simulated Data

Waveform		
Carrier frequency	f_c	10 GHz
Bandwidth	B	1 GHz
Range resolution	δ_R	0.15 m
PRI	T_r	1 ms
Ambiguity velocity	V_a	15 m/s
Pulses	M	32
Migration per ambiguity in δ_R	μ_a	3.2
Processing parameters		
Range cells in LRRS	K	6
Number of ambiguities	N_a	3
Maximum velocity	$V_{\max}$	22.5 m/s

IV. PERFORMANCE ASSESSMENT

Due to iterative nature of the developed algorithms, it is not possible to derive their performance analytically. Instead, we employ Monte-Carlo simulations to evaluate the performance of the presented techniques. All the simulations within this section are done with the radar parameters given in Table I. Also, for all the simulations, we exploit the true structure of CM in slow-time $\mathbf{M_v}$, known *a priori* and identical for all the range cells within the LRRS.

An important question is the initialization of the algorithms, which can affect their performance. In particular, it can influence the number of iterations required for convergence. Recall that in both cases the iterative procedure is applied to obtain an estimation of $\hat{\alpha}$ present in the scene under H_1, see (16) and (28). In this light, both algorithms should be initialized with some noniterative estimation of $\hat{\alpha}$. As was stated before, noniterative estimation of $\hat{\alpha}$ exists only in case of no texture variation within LRRS (locally Gaussian assumption) and it is given by: $\hat{\alpha} = \mathbf{a}^H \mathbf{M^{-1}} \mathbf{y} / \mathbf{a}^H \mathbf{M^{-1}} \mathbf{a}$, where $\tau_k = 1$, $\forall k \in \mathcal{K}$. The other strategy efficient under both hypotheses would be to use for initialization in each range cell the power estimated at the previous angle scan (similar to the clutter map technique [11]), especially if the PDF of the texture is unknown *a priori*. Good initial estimation will result in fast convergence of the algorithm, assuming clutter power does not vary significantly from scan to scan.

In view of the foregoing we study the ability of the proposed techniques to keep P_{FA} at the designed level. In particular, the number of iterations required to perform CFAR detection is of interest. In order to check the ability of the algorithms to keep the designed P_{FA}, detection is applied to a target-free scene. Therefore, we initialize both algorithms with $\hat{\alpha} = \mathbf{a}^H \mathbf{M^{-1}} \mathbf{y} / \mathbf{a}^H \mathbf{M^{-1}} \mathbf{a}$ and apply AM (27) and maximum likelihood (ML) (17) algorithms with *a priori* known PDF of clutter texture.

For the simulations herein, we focus on K-distributed clutter with shape parameter $\nu = 0.5$ or, equivalently, the exponentially distributed clutter, with known CM and white spectrum in slow-time $\mathbf{M_v} = \mathbf{I}$ [37]. The ability of ML and AM algorithms to keep the designed P_{FA} [used to

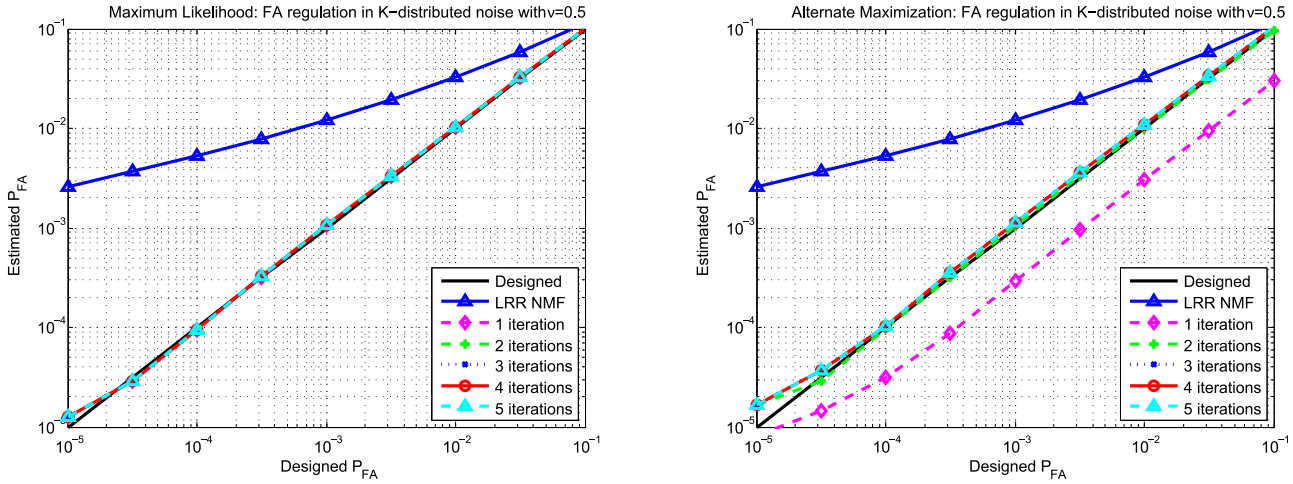

Fig. 3. False alarm regulation in K-distributed clutter, $\nu = 0.5$: (a) Maximum likelihood algorithm, (b) alternate maximization algorithm.

set the threshold according to (34)], is estimated from 10^3 Monte-Carlo trials and shown in Fig. 3. For each trial ,P_{FA} is evaluated over all range-velocity hypotheses, thus in $K \times (MN_a) = 576$ cells. False alarm regulation of NMF applied to an LRRS (LRR NMF) (8) is added for comparison to the plots. The performance of LRR NMF shows that wrong assumption on texture variation within LRRS results in unsatisfactory degradation of P_{FA}. On the other hand, ML algorithm provides designed P_{FA} already after the first iteration, given the shape parameter of K-distribution is known. Similar result is obtained with AM algorithm after two iterations without prior knowledge of the clutter PDF. In practice, the PDF of clutter is unknown, but it can be estimated from data in homogeneous environment, resulting in a faster convergence of the detector. If a reliable estimation of texture PDF cannot be retrieved from the data due to fast-varying radar scene, such as urban environment, AM approach provides a more attractive solution. Thus, the choice between two algorithms should be done based on prior knowledge of the texture and tractability of calculation the functions $c_M(x)$ and $h_M(x)$.

The analysis presented above consider fixed clutter shape parameter ν. Similarly to results for CM estimation [25], we expect that the number of iterations for convergence of the algorithms depends on the clutter shape. In order to prove this statement, the ratio of the estimated P_{FA} to designed P_{FA} is evaluated via Monte-Carlo routine for the threshold corresponding to $P_{FA} = 10^{-3}$. Independently of clutter shape parameter, ML algorithm becomes CFAR detector after one iteration. At the same time, the number of iterations in AM algorithm depends on the clutter shape parameter ν, as proved by simulations in Fig. 4. The plots show that for practical values of $\nu = 0.5 \div 10$, two iterations of AM algorithm are enough for convergence. This value is used for further simulations.

The other important characteristic of CFAR is the detection probability. Two crucial factors influence detection

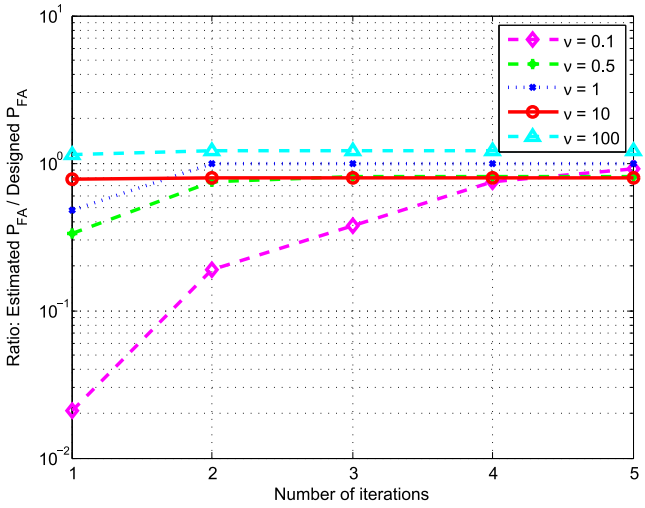

Fig. 4. False alarm loss of alternate maximization algorithm versus iterations.

performance: correct model of clutter and representative model of target motion. Incorrect model of clutter results in a detector not satisfying CFAR property, as shown above. On the other hand, to avoid iterative techniques, one can ignore the migration term in target model (2) and apply NMF for every range cell. Note that this approach preserves P_{FA} at the designed level. For example, consider a target with $v_0 = 0.5V_a$ (where $V_a = c/(2f_cT_r)$ is the radar ambiguous velocity), which migrates $\mu|_{0.5V_a} = 1.6$ range cells during CPI. As in the previous simulations, we consider K-distributed clutter with shape parameter $\nu = 0.5$. In Fig. 5, the detection performance of NMF applied to one range cell with narrow-band target signature (NB NMF) is compared with the two proposed techniques (AM and ML) together with the clairvoyant detector. Clairvoyant detector is implemented via GLRT (25) using known values of α and σ_C^2. The horizontal axis shows SCR after coherent

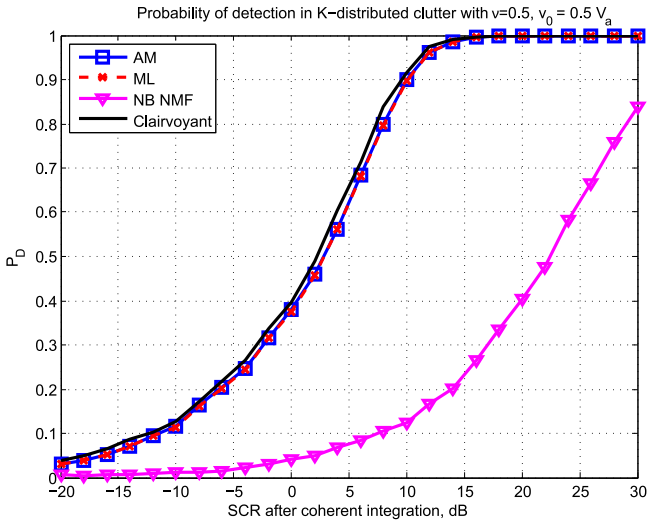

Fig. 5. Detection probability of a migrating target in K-distributed clutter with $\nu = 0.5$ using different algorithms, $v_0 = 0.5V_a$, $P_{FA} = 10^{-6}$.

integration. The detection curves of all the algorithms are obtained via Monte-Carlo routine. The results clearly show that not accounting for target migration results in severe loss in the detection performance. This loss diminishes for slow targets and increases for fast-moving targets proportionally to the smearing of the target due to migration.

By the wideband assumption, a moving target migrates through a number of range cells conditional on its velocity. If the clutter texture in these range cells varies rapidly over range, a fast target will experience diverse interference within CPI. Contrary, a slow and therefore nonmigrating target will be present in one range cell during the whole CPI [see Fig. 1(a) and (b)]. Such an implicit averaging of the clutter texture, intrinsic for a migrating target, suggests that the detection performance of a migrating target will be velocity-dependent in inhomogeneous clutter. On the contrary, this phenomenon does not exist for nonmigrating targets, where the detection performance in spectrally white clutter (or noise) does not depend on the velocity of the target. This effect is similar to performance improvement of an extended target compared to a point target [12], [28]. The major difference between the two models is that for range migrating target, its signature is summed up coherently along the range walk, while the responses of a range-extended target are integrated incoherently along range.

The detection performance is studied in Fig. 6 using AM algorithm with $P_{FA} = 10^{-6}$ and wideband target signature; the horizontal axis shows SCR after coherent integration. The ML algorithm shows identical performance and therefore it is not plotted. By definition of target model, the test for a target with $v = 0$ is equivalent to NMF applied for one range cell. Note the improvement in detection of a fast target ($v_0 = 1.5V_a$, which migrates $\mu|_{1.5V_a} = 4.8$ range cells) with respect to the nonmigrating target is about 8 dB for clutter with shape parameter $\nu = 0.5$. Let us remark that the P_d curves in Fig. 6, corresponding to different values

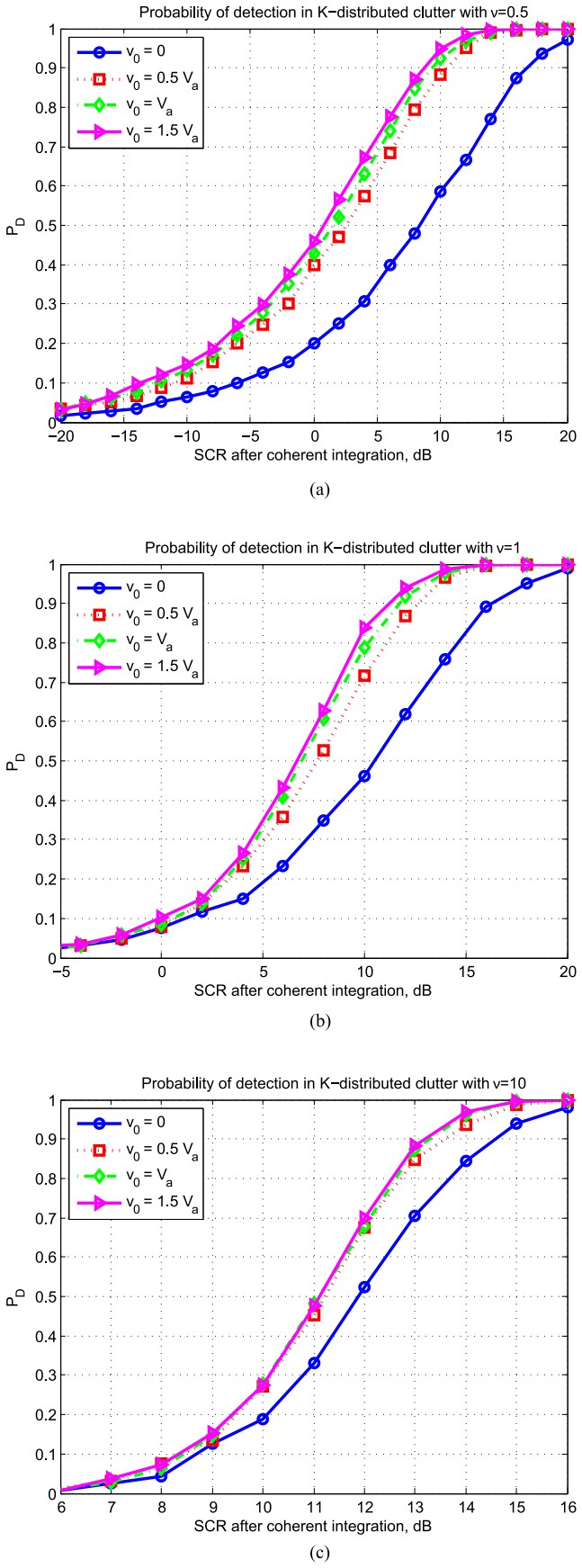

Fig. 6. Detection probability of alternate maximization and maximum likelihood algorithms for a target with different velocity, $P_{FA} = 10^{-6}$ and clutter shape parameter (a) $\nu = 0.5$; (b) $\nu = 1$; (c) $\nu = 10$.

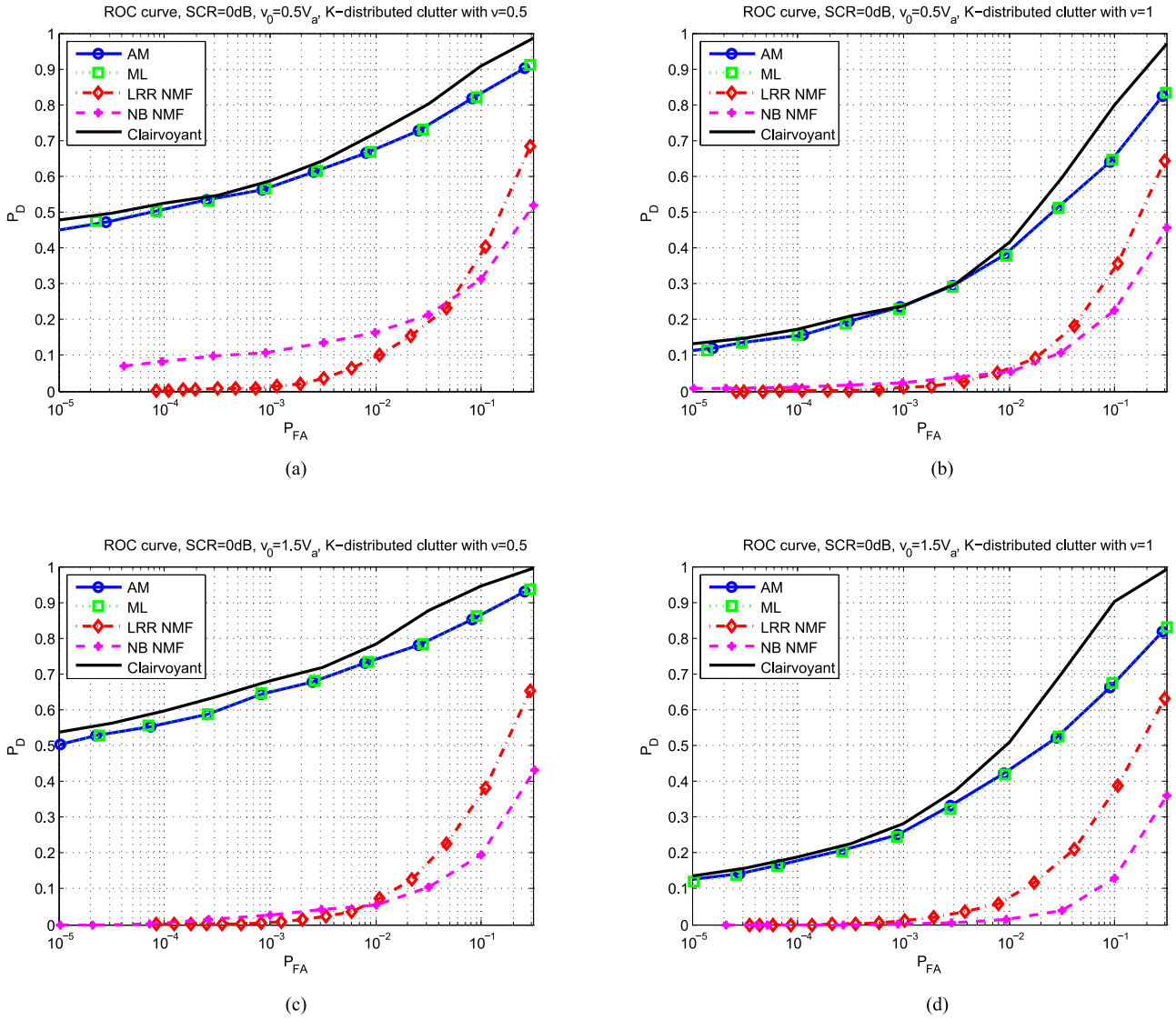

Fig. 7. ROC curves for a target with $SCR = 0$ dB after coherent integration in K-distributed clutter: (a) $v_0 = 0.5V_a$, $\nu = 0.5$; (b) $v_0 = 0.5V_a$, $\nu = 1$; (c) $v_0 = 1.5V_a$, $\nu = 0.5$; (d) $v_0 = 1.5V_a$, $\nu = 1$.

of clutter shape parameter, have different SCR scale. The presented results emphasize that the detection performance depends on target velocity more in case of spiky clutter and this effect gradually vanishes as ν increases. In the limiting case $\nu \to +\infty$, the clutter is locally Gaussian and the detection performance does not depend on target velocity.

To emphasize the advantages of the proposed techniques with respect to the existing approaches, we estimate their performance in terms of ROC curves. In particular, we focus on a weak target scenario in highly inhomogeneous and spiky clutter. For comparison, we consider all the detectors discussed above, namely: ML, AM, LRR NMF, NB NMF, and the clairvoyant detector. For performance assessment, we simulate a target with SCR = 0 dB after coherent integration moving with velocity $v_0 = 0.5V_a$ or $v_0 = 1.5V_a$ embedded in a K-distributed clutter. Also, we consider two values of clutter shape parameter: $\nu = 0.5$ and $\nu = 1$. Simulation results are shown in Fig. 7, each plot corresponds to a specific combination of ν and v_0. The results show significant improvement of the proposed techniques with respect to LRR NMF and NB NMF. Note the different nature of performance degradation of these algorithms: LRR NMF suffers from the incorrect model of clutter and therefore loses CFAR property. Contrary, NB NMF keeps CFAR property, but brings significant loss in detection because of inaccurate target signature. On the other hand, the loss of the AM and ML algorithms with respect to the clairvoyant detector is negligible. The comparison of the plots with equal clutter shape parameter allows to see the benefits of a fast-moving target detection over slow one in highly inhomogeneous compound-Gaussian clutter, already mentioned above.

V. CONCLUSION

In this paper, we discussed the problem of fast-moving target detection with wideband radar, providing range resolution of an order of 1 m or higher. In particular, we focused

on the migration effect essential for fast-moving targets, observed by such radars, and exploited it to perform detection in highly inhomogeneous compound-Gaussian clutter. We proposed two detection algorithms which use iterative procedure for amplitude estimation and converges in one or two iterations for practical scenarios. Accounting for range migration results in significant (up to 8 dB) improvement for fast-moving target detection for realistic spiky clutter. An additional improvement with respect to the narrow-band Doppler processing is achieved by correct migration compensation of fast-moving targets. The proposed AM algorithm seems more attractive for practical application since it does not require any knowledge of clutter PDF and can be implemented on a chain identical to the one used for CM estimation in compound-Gaussian clutter.

APPENDIX

Herein, we prove the local convergence of the amplitude estimator (22), which is a part of the proposed distribution-free detector for range migrating target in an inhomogeneous environment. The iterative amplitude estimation has general form of the fixed point estimator $\hat{\alpha}_i = g(\hat{\alpha}_{i-1})$. The fixed point estimator converges locally at point $\hat{\alpha}_{FP}$ if the function g satisfies [38]:

$$\left|g'(\hat{\alpha}_{\mathrm{FP}})\right| < 1 \tag{35}$$

with $\hat{\alpha}_{\mathrm{FP}} = \hat{\alpha}_\infty = g(\hat{\alpha}_\infty)$.

In order to prove this, we can write from (22):

$$g(\hat{\alpha}) = \frac{\sum_{k=0}^{K-1} \frac{\mathbf{a_k}^H \mathbf{M_v^{-1}} \mathbf{y_k}}{(\mathbf{y_k}-\hat{\alpha}\mathbf{a_k})^H \mathbf{M_v^{-1}} (\mathbf{y_k}-\hat{\alpha}\mathbf{a_k})}}{\sum_{k=0}^{K-1} \frac{\mathbf{a_k}^H \mathbf{M_v^{-1}} \mathbf{a_k}}{(\mathbf{y_k}-\hat{\alpha}\mathbf{a_k})^H \mathbf{M_v^{-1}} (\mathbf{y_k}-\hat{\alpha}\mathbf{a_k})}} = \frac{\sum_{k=0}^{K-1} n_k}{\sum_{k=0}^{K-1} d_k} \tag{36}$$

and take the derivative. Herein, for derivatives of complex functions, we use the strategy described in [39]; especially, when taking the partial derivative over $\hat{\alpha}$, we consider $\hat{\alpha}^*$ to be a constant (the sign * states for complex conjugate). Then

$$n_k' = n_k n_k^* - \hat{\alpha}^* n_k d_k, \tag{37}$$

$$d_k' = d_k n_k^* - \hat{\alpha}^* d_k^2 \tag{38}$$

and the derivative at the fixed point is

$$g'(\hat{\alpha}_{\mathrm{FP}}) = \frac{\sum_{k=0}^{K-1} |n_k - \hat{\alpha}_{\mathrm{FP}} d_k|^2}{\sum_{k=0}^{K-1} d_k}. \tag{39}$$

Taking into account that d_k is a real-valued function as a ratio of quadratic forms, the requirement on convergence (35) can be given by

$$\left|g'(\hat{\alpha}_{\mathrm{FP}})\right| = \frac{\sum_{k=0}^{K-1} |n_k - \hat{\alpha}_{\mathrm{FP}} d_k|^2}{\sum_{k=0}^{K-1} d_k} < 1. \tag{40}$$

Inequality (40) holds, if $\forall k \in \mathcal{K}$, such that $d_k > 0$:

$$d_k \left|\hat{\alpha}_{\mathrm{FP}} - \frac{n_k}{d_k}\right|^2 < 1. \tag{41}$$

Note that the requirement $d_k > 0$ is necessary to cover the situation with nonmigrating target, when at least one substeering vector $\mathbf{a_k}$ appears to be zero vector (in the range cells not including the target signature).

To proceed further, we denote amplitude estimation from the data in the kth range cell by $\hat{\alpha}_k = n_k/d_k$. Then, in terms of (36), the last inequality can be given by

$$\frac{\mathbf{a_k}^H \mathbf{M_v^{-1}} \mathbf{a_k} \, |\hat{\alpha}_{\mathrm{FP}} - \hat{\alpha}_k|^2}{(\mathbf{y_k} - \hat{\alpha}_{\mathrm{FP}}\mathbf{a_k})^H \mathbf{M_v^{-1}} (\mathbf{y_k} - \hat{\alpha}_{\mathrm{FP}}\mathbf{a_k})} < 1. \tag{42}$$

After simple mathematical derivations, the condition on convergence is given by

$$\frac{|\hat{\alpha}_{\mathrm{FP}} - \hat{\alpha}_k|^2}{|\hat{\alpha}_{\mathrm{FP}} - \hat{\alpha}_k|^2 + \frac{\mathbf{y_k^H M_v^{-1} y_k}}{\mathbf{a_k^H M_v^{-1} a_k}} \left(1 - \frac{|\mathbf{a_k^H M_v^{-1} y_k}|^2}{(\mathbf{a_k^H M_v^{-1} a_k})(\mathbf{y_k^H M_v^{-1} y_k})}\right)} < 1 \tag{43}$$

where the second item in the denominator is a nonnegative value independent of $\hat{\alpha}$. In fact, for nonzero variance of clutter in every range cell ($\sigma_k^2 > 0$), these value is positive and therefore the condition (35) is satisfied. Q.E.D.

ACKNOWLEDGMENT

The authors would like to thank the anonymous reviewers for their valuable comments, which helped to improve the paper. The authors would also like to thank N. Bogdanović, S. Bidon, and J.-P. Ovarlez for the fruitful discussions.

REFERENCES

[1] F. Le Chevalier
Principles of Radar and Sonar Signal Processing. Norwood, MA, USA: Artech House, 2002.

[2] N. Jiang, R. Wu, and J. Li
Super resolution feature extraction of moving targets
IEEE Trans. Aerosp. Electron. Syst., vol. 37, no. 3, pp. 781–793, Jul. 2001.

[3] R. Perry, R. Dipietro, and R. Fante
SAR imaging of moving targets
IEEE Trans. Aerosp. Electron. Syst., vol. 35, no. 1, pp. 188–200, Jan. 1999.

[4] S. Bidon, L. Savy, and F. Deudon
Fast coherent integration for migrating targets with velocity ambiguity
In *Proc. 2011 IEEE RadarCon*, 2011, pp. 027–032.

[5] J. Xu, J. Yu, Y.-N. Peng, and X.-G. Xia
Radon-Fourier transform for radar target detection, I: Generalized Doppler filter bank
IEEE Trans. Aerosp. Electron. Syst., vol. 47, no. 2, pp. 1186–1202, Apr. 2011.

[6] F. Le Chevalier, O. Krasnov, F. Deudon, and S. Bidon
Clutter suppression for moving targets detection with wideband radar
In *Proc. 2011 Eur. Signal Process. Conf.*, 2011, pp. 427–430.

[7] F. Deudon, S. Bidon, O. Besson, and J. Tourneret
Velocity dealiased spectral estimators of range migrating targets using a single low-PRF wideband waveform
IEEE Trans. Aerosp. Electron. Syst., vol. 49, no. 1, pp. 244–265, Jan. 2013.

[8] S. Bidon, J.-Y. Tourneret, L. Savy, and F. Le Chevalier
Bayesian sparse estimation of migrating targets for wideband radar
IEEE Trans. Aerosp. Electron. Syst., vol. 50, no. 2, pp. 871–886, Apr. 2014.

[9] N. Petrov and F. Le Chevalier
Iterative adaptive approach for unambiguous wideband radar target detection
In *Proc. 2015 Eur. Radar Conf.*, Sep. 2015, pp. 45–48.

[10] Q. Li, E. J. Rothwell, K.-M. Chen, and D. P. Nyquist
Scattering center analysis of radar targets using fitting scheme and genetic algorithm
IEEE Trans. Antennas Propag., vol. 44, no. 2, pp. 198–207, Feb. 1996.

[11] M. A. Richards, J. A. Scheer, W. A. Holm, and W. L. Melvin
Principles of Modern Radar. Raleigh, NC, USA: SciTech Pub., 2010.

[12] E. Conte, A. d. Maio, and G. Ricci
CFAR detection of distributed targets in non-Gaussian disturbance
IEEE Trans. Aerosp. Electron. Syst., vol. 38, no. 2, pp. 612–621, Apr. 2002.

[13] A. De Maio and M. Greco
Modern Radar Detection Theory. Raleigh, NC, USA: SciTech Pub., 2016.

[14] S. Watts
Radar detection prediction in K-distributed sea clutter and thermal noise
IEEE Trans. Aerosp. Electron. Syst., vol. AES-23, no. 1, pp. 40–45, Jan. 1987.

[15] A. Farina, F. Gini, M. Greco, and L. Verrazzani
High resolution sea clutter data: statistical analysis of recorded live data
In *Proc. IEE Proc. Radar, Sonar Navig.*, vol. 144, no. 3, pp. 121–130, 1997.

[16] N. Pulsone and R. Raghavan
Analysis of an adaptive CFAR detector in non-Gaussian interference
IEEE Trans. Aerosp. Electron. Syst., vol. 35, no. 3, pp. 903–916, Jul. 1999.

[17] M. S. Greco and F. Gini
Statistical analysis of high-resolution SAR ground clutter data
IEEE Trans. Geosci. Remote Sens., vol. 45, no. 3, pp. 566–575, Mar. 2007.

[18] F. Pascal, P. Forster, J.-P. Ovarlez, and P. Larzabal
Performance analysis of covariance matrix estimates in impulsive noise
IEEE Trans. Signal Process., vol. 56, no. 6, pp. 2206–2217, Jun. 2008.

[19] F. Pascal, Y. Chitour, J.-P. Ovarlez, P. Forster, and P. Larzabal
Covariance structure maximum-likelihood estimates in compound Gaussian noise: Existence and algorithm analysis
IEEE Trans. Signal Process., vol. 56, no. 1, pp. 34–48, Jan. 2008.

[20] K. D. Ward, S. Watts, and R. J. Tough
Sea Clutter: Scattering, the K Distribution and Radar Performance, vol. 20. London, U.K.: IET, 2006.

[21] K. J. Sangston, F. Gini, M. V. Greco, and A. Farina
Structures for radar detection in compound Gaussian clutter
IEEE Trans. Aerosp. Electron. Syst., vol. 35, no. 2, pp. 445–458, Apr. 1999.

[22] E. Jay, J. P. Ovarlez, D. Declercq, and P. Duvaut
BORD: Bayesian optimum radar detector
Signal Process., vol. 83, no. 6, pp. 1151–1162, 2003.

[23] E. Conte, M. Lops, and G. Ricci
Asymptotically optimum radar detection in compound-gaussian clutter
IEEE Trans. Aerosp. Electron. Syst., vol. 31, no. 2, pp. 617–625, Apr. 1995.

[24] F. Gini
Sub-optimum coherent radar detection in a mixture of K-distributed and Gaussian clutter
In *IEE Proc. Radar, Sonar Navig.*, vol. 144, no. 1, pp. 39–48, 1997.

[25] F. Gini and M. Greco
Covariance matrix estimation for CFAR detection in correlated heavy tailed clutter
Signal Process., vol. 82, no. 12, pp. 1847–1859, 2002.

[26] F. Pascal, J.-P. Ovarlez, P. Forster, and P. Larzabal
Constant false alarm rate detection in spherically invariant random processes
In *Proc. 2004 Eur. Signal Process. Conf.*, 2004, pp. 2143–2146.

[27] E. Conte, A. De Maio, and G. Ricci
Recursive estimation of the covariance matrix of a compound-Gaussian process and its application to adaptive CFAR detection
IEEE Trans. Signal Process., vol. 50, no. 8, pp. 1908–1915, Aug. 2002.

[28] K. Gerlach
Spatially distributed target detection in non-Gaussian clutter
IEEE Trans. Aerosp. Electron. Syst., vol. 35, no. 3, pp. 926–934, Jul. 1999.

[29] J. Yu, J. Xu, Y.-N. Peng, and X.-G. Xia
Radon-Fourier transform for radar target detection (III): Optimality and fast implementations
IEEE Trans. Aerosp. Electron. Syst., vol. 48, no. 2, pp. 991–1004, Apr. 2012.

[30] F. Dai, H. Liu, P. Shui, and S. Wu
Adaptive detection of wideband radar range spread targets with range walking in clutter
IEEE Trans. Aerosp. Electron. Syst., vol. 48, no. 3, pp. 2052–2064, Jul. 2012.

[31] S. M. Kay
Fundamentals of Statistical Signal Processing, vol. II: Detection Theory. Englewood Cliffs, NJ, USA: Prentice-Hall, 1998.

[32] S. Kraut and L. Scharf
The CFAR adaptive subspace detector is a scale-invariant GLRT
IEEE Trans. Signal Process., vol. 47, no. 9, pp. 2538–2541, Sep. 1999.

[33] E. Conte and M. Longo
Characterisation of radar clutter as a spherically invariant random process
IEE Proc. Commun., Radar Signal Process., vol. 134, no. 2, pp. 191–197, 1987.

[34] I. S. Gradshteyn and I. M. Ryzhik
Tables of Integrals, Series, and Products. New York, NY, USA: Academic, 2000.

[35] E. Conte and A. De Maio
Mitigation techniques for non-Gaussian sea clutter
IEEE J. Ocean. Eng., vol. 29, no. 2, pp. 284–302, Apr. 2004.

[36] A. O. Steinhardt
Enhanced convergence adaptive detection
DTIC, Tech. Rep. AFOSR 91-0149, Cornell Univ., Dept. Elect. Eng., 324 Engr. Theory Center Building, Ithaca, NY 14853–3801, 1993.

[37] E. Conte, M. Longo, and M. Lops
Modelling and simulation of non-Rayleigh radar clutter
IEE Proc. Radar Signal Process., vol. 138, no. 2, pp. 121–130, 1991.

[38] J. Bak and D. J. Newman
Complex Analysis. New York, NY, USA: Springer, 2010.

[39] S. M. Kay
Fundamentals of Statistical Signal Processing, vol. I: Estimation Theory. Englewood Cliffs, NJ, USA: Prentice-Hall, 1993.

Nikita Petrov graduated with the engineering degree in radio-electronic control systems from the Baltic State Technical University "VOENMEH," Saint-Petersburg, Russia, in 2012. He is currently working toward the Ph.D. degree on signal processing techniques for moving target detection with wideband radar systems at Delft University of Technology, Delft, The Netherlands.

His graduation project and further research activities in the scientific center "Leninetz," Saint-Petersburg, were focused on radar imaging with high-resolution airborne SAR systems. In 2013, he joined the Microwave Sensing, Signals and Systems group at Delft University of Technology

Francóis Le Chevalier received the degree from Ingénieur Civil des Télécommunications, Telecom Paristech, in 1974. He is an Emeritus Professor at Delft University of Technology, Delft, The Netherlands, and a retired Chief Scientist of Thales, Land & Air Systems. He is an author of many papers, tutorials, and patents in radar and electronic warfare, he is the author of a book *Radar and Sonar Signal Processing Principles* (Artech House, 2002), editor of *Non-Standard Antennas* (Wiley, 2010), co-author of *Waveform Design and Diversity for Advanced Radar Systems* (Chapter 13) (IET Radar, Sonar and Navigation series, 2012), co-author of *Principles of Modern Radar: Advanced Techniques* (Chapter 11) (Scitech, IET Publishing, 2012), and co-author of *Advanced Ultrawideband Radar: Signals, Targets, and Applications* (Chapter 12) (CRC Press, December 2016). A French pioneer in adaptive digital beamforming and STAP radar systems demonstrations, his current research activities include space-time coding for active antenna systems, and wideband unambiguous radar systems.

Prof. Le Chevalier has been active in, or chairing, the Technical Program Committees of most IEEE International Radar Conferences since Brest, 1999, has recently chaired the Technical Program Committee of EURAD 2012, Amsterdam, and was the Honorary Chair of SEE/IEEE International Radar Conference in France, 2014.

Alexander G. Yarovoy (F'15) received the Diploma (Hons.) degree in radiophysics and electronics from the Kharkov State University, Kharkov, Ukraine, in 1984, and the Candidate Physics & Mathematics Science and Doctor Physics & Mathematics Science degrees in radiophysics from Kharkov State University, Kharkov, Ukraine, in 1987 and 1994, respectively.

In 1987, he joined the Department of Radiophysics, Kharkov State University, as a Researcher, and in 1997 became a Professor. From September 1994 to 1996, he was with the Technical University of Ilmenau, Ilmenau, Germany, as a Visiting Researcher. Since 1999, he has been with the Delft University of Technology, Delft, The Netherlands. Since 2009 he leads there a chair of Microwave Sensing, Systems and Signals. His main research interests include (ultra-)wideband radar, microwave imaging, and applied electromagnetics (in particular, UWB antennas). He has authored and co-authored more than 450 scientific or technical papers, 4 patents, and 14 book chapters.

Prof. Yarovoy received the European Microwave Week Radar Award for the paper that best advances the state-of-the-art in radar technology in 2001 (together with L. P. Ligthart and P. van Genderen) and in 2012 (together with T. Savelyev). In 2010, together with D. Caratelli Prof. Yarovoy received the best paper award of the Applied Computational Electromagnetic Society (ACES). He served as a Guest Editor of five special issues of the IEEE Transactions and other journals. He also served as the Chair and TPC Chair of the 5th European Radar Conference (EuRAD08), Amsterdam, The Netherlands, as well as the Secretary of the 1st European Radar Conference (EuRAD04), Amsterdam, The Netherlands, also as the Co-Chair and TPC Chair of the Xth International Conference on GPR (GPR2004), Delft. Since 2008, he has been serving as the Director of the European Microwave Association (EuMA).